J Mater Sci (2010) 45:6455–6460
DOI 10.1007/s10853-010-4731-x

Influence of the shapes on the magnetic and electrical transport properties of $La_{2/3}Ca_{1/3}MnO_3$ nanoparticles

J. C. Riaño-Rojas · E. Restrepo-Parra · G. Orozco-Hernández · J. A. Urrea-Serna · J. Restrepo

Received: 30 November 2009 / Accepted: 21 June 2010 / Published online: 2 July 2010

Abstract In this work, the role of the geometrical shape, using the Minkowski's metrics, upon the temperature dependence of the magnetic and electrical transport properties of $La_{2/3}Ca_{1/3}MnO_3$ nanoparticles was carried out. We considered a set of small particles with different shapes containing approximately the same amount of Mn ions ($\sim$6500) and distributed as a simple cubic structure in agreement with the manganites perovskite structure. The model is based on the standard Monte Carlo–Metropolis method and the classical Heisenberg Hamiltonian involving nearest magnetic neighbors interactions. Results dealing with the dependence of the Curie temperature for nanoparticles is lower than material in bulk. Moreover, magnetization and magnetic susceptibility as a function of the metric for some field cooled values. As the field cooled increased the transition temperature T_C increased. On the other hand, low temperature coercive force and resistivity with the shape of the nanoparticles, having different metric parameters, are present and discussed.

J. C. Riaño-Rojas
Departamento de Matemáticas y Estadística, Universidad Nacional de Colombia, Sede Manizales, A.A. 127, Manizales, Colombia

E. Restrepo-Parra (✉) · G. Orozco-Hernández · J. A. Urrea-Serna
Departamento de Física y Química, Universidad Nacional de Colombia, Sede Manizales, A.A. 127, Manizales, Colombia
e-mail: erestrepopa@unal.edu.co

J. Restrepo
Grupo de Magnetismo y Simulación G+, Instituto de Física, Universidad de Antioquia, A.A. 1226, Medellín, Colombia

Introduction

As is well established the behavior of magnetic particles in the submicron range is strongly dependent on size and shape. In particular, this last feature has been important as far as new advances in sample preparation methods and suitable synthesis routes can lead to different geometric confinements for which different physical properties can be found. On this respect it is worth to mention the current progress in the so-called patterned systems employing the top–down approach where nanostructures with different geometric shapes have been successfully developed [1]. Patterned nanomagnets are being already used for instance in the development of magnetoresistive random access memories (MRAMs) and ultrahigh density patterned recording media where proper choices of size and shape are crucial in capturing unique magnetoelectronic properties [2–4].

The influence of shape on the magnetic properties of nanomagnets namely: elliptical [5, 6], triangular [7], square [8–11], circular [12, 13], nanorings [14] and diamond-shaped [15], among others, have been investigated. However, most of such studies stress on (i) flat nanomagnets having bidimensional features and (ii) soft magnetic behavior, such permalloys, in which magnetocrystalline anisotropy is much weaker compared to exchange interaction and magnetostatic energy. Contrary to this we report in this work on the shape effect, quantified through the Minkowski's metrics, upon the magnetic and electron transport properties of $La_{2/3}Ca_{1/3}MnO_3$ manganites nanoparticles with a rather magnetically hard behavior, i.e. magnetostatic energy is negligible compared to exchange interaction and magnetocrystalline anisotropy. Manganites have been systematically investigated in the form of bulk, thin films and nanoparticles, due to their unique properties and potential

technological applications [16–18] and only some few reports dealing with geometrical features in manganites nanoparticles have been carried out [19].

In this work, we address the effect of geometry on the magnetic, hysteretic and electrical transport properties, of ferromagnetic (FM) $La_{2/3}Ca_{1/3}MnO_3$ nanoparticles. We use the Monte Carlo method implemented with a single-spin movement Metropolis algorithm, in the framework of a three-dimensional classical Heisenberg model, including nearest magnetic neighbors superexchange interactions, magnetocrystalline anisotropy and a Zeeman term for simulation of the hysteresis loops. Electronic transport properties are investigated using the Kronig–Penney model.

Model description

The manganite $La_{2/3}Ca_{1/3}MnO_3$ is ferromagnetic below 260 K, which is the highest critical temperature of this material [20]. It has a perovskite type structure where Mn magnetic ions are arranged following a simple cubic crystalline structure [21]. It is characterized for having three types of Mn magnetic ions corresponding to Mn^{4+} ($S = 3/2$), which are bonded to Ca^{2+} ions, Mn^{3+eg} and $Mn^{3+eg'}$ ($S = 2$) that are related to La^{3+}. In our simulation an array of Mn ions with orbital ordering as proposed by Hotta et al. [22] was used. We have carefully chosen several nanoparticles having approximately the same amount of atoms ($\sim$6500 Mn ions) but having different geometrical shapes depending on the metrics.

Free boundary conditions were implemented and the model employed was based on a three-dimensional classical Heisenberg Hamiltonian including terms of exchange coupling between nearest magnetic neighbors, single ion site surface anisotropy, cubic magnetocrystalline anisotropy for core ions, and a Zeeman term accounting for the interaction of the spins with a uniform external applied magnetic field [23]. Magnetic ions $Mn^{3+eg'}$, Mn^{3+eg} and Mn^{4+d3} are represented by classical Heisenberg spins with different magnitudes according to their corresponding electronic configurations. The Hamiltonian employed reads as follows:

$$H = -\sum_{i\neq j} J_{ij}\vec{S}_i \cdot \vec{S}_j - K_B \sum_i (S_i \cdot \hat{a})^2 - K_S(S_i \cdot \hat{n}_i) - h\sum_i \vec{S}_i \cdot \hat{h} \quad (1)$$

Here K_B and K_S stand for the anisotropy constants of the core and the surface ions, respectively. In this work we use the value $K_B \approx 1.2484$ meV/nm^3 [24], that is considered in the (100) crystallographic plane direction as was reported in a previous work [19]. For the surface anisotropy constant we have assumed $K_B/K_S = 1$. The unit vector $\hat{a}$ indicates the easy axis (100) direction for only core ions. On the other hand unit vectors $\hat{n}$ on the surface, calculated at each ith-Mn position, for single ion site surface anisotropy, were computed according to [19, 25]:

$$\hat{n}_{i\neq j} = \sum_{i\neq j}\left(\vec{d}_j - \vec{d}_i\right) \Big/ \left|\sum_{i\neq j}\left(\vec{d}_j - \vec{d}_i\right)\right| \quad (2)$$

where the sum runs over the jth nearest magnetic neighbors with position $\vec{d_j}$ around each ith-Mn ion. Figure 1 presents nanoparticles shape including the surface unit vectors $\hat{n}$, obtained with Eq. 2. These vectors reflex the influence of the surface anisotropy on the Hamiltonian.

Three types of bonds were considered: $Mn^{3+eg'}$–O–Mn^{3+eg}, Mn^{3+eg}–O–Mn^{4+d3} and $Mn^{3+eg'}$–O–Mn^{4+d3} with superexchange parameters J_1, J_2 and J_3, respectively [18]. Numerical values for these parameters were set to

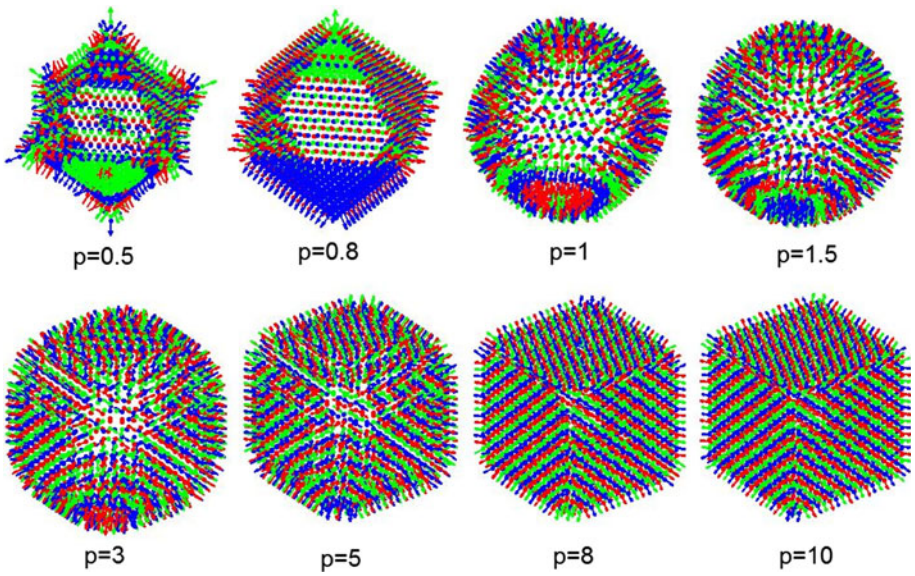

Fig. 1 Different nanoparticle shapes corresponding to different metrics values. Surface anisotropy unit vectors are shown

$J_1 = 4.65$ meV, $J_2 = 3J_{ab1} = 7.7$ meV and $J_3 = 1.35$ meV [18], which were fitted to reproduce the Curie temperature (~ 260 K) for this system under bulk conditions.

This Hamiltonian is based on the adiabatic approximation that stands that electrons and ions can be treated separately with a small perturbation from the lattice [26]. Then, the electron–phonon interaction is neglected. Although many authors have been considered this interaction, other authors as Okamoto et al. [27] that carried out electron–electron and electron-lattice interaction studies in manganites, concluded that the characteristic energy of the orbital interaction is much higher than that of the lattice vibration.

On the other hand, a single-spin movement Metropolis–Monte Carlo algorithm was used for obtaining the equilibrium thermodynamic properties, namely magnetization, energy, specific heat and magnetic susceptibility. Around 2×10^4 Monte Carlo steps per spin (mcs) were considered in computing canonical averages and around 10^4 mcs were discarded for equilibration.

In order to generate the different shapes, the Minkowski's metrics, giving the non-Euclidean distance between two points, was employed [28]:

$$d_p(x,y) = \left\{ \sum_{j=1}^{n} |x_j - y_j|^p \right\}^{1/p} \quad (3)$$

where $d_p(x,y)$ is the distance between points x and y, n is the size of (x, y) vectors, j runs over all vector elements and p is the metrics parameter (if $0 < p < 1$ it is named seudometric). Figure 1 shows the shapes used in this work. They were obtained varying the p parameter as 0.5, 0.8, 1, 1.5, 2, 3, 5, 8 and 10. The following important geometrical features are observed:

(a) if $0 < p < 1$, the nanoparticle edges are hyperbolic,
(b) if $p = 1$, the nanoparticle has octahedrical shape,
(c) if $p = 2$, the nanoparticle has spherical shape (Euclidean metrics) and
(d) if p tends to infinity, the nanoparticle tends to a cubic shape.

Magnetic and hysteretic properties were simulated according to the model proposed by Riaño-Rojas et. al. [19], and resistivity was determined on the basis of the Kronig–Penney model reported by Vandewalle et al. [29].

Results and discussion

Figure 2 shows the temperature dependence of both the magnetization per site and magnetic susceptibility at zero magnetic field cooled, for nanoparticles built at different metrics values and therefore different shapes. The magnetic

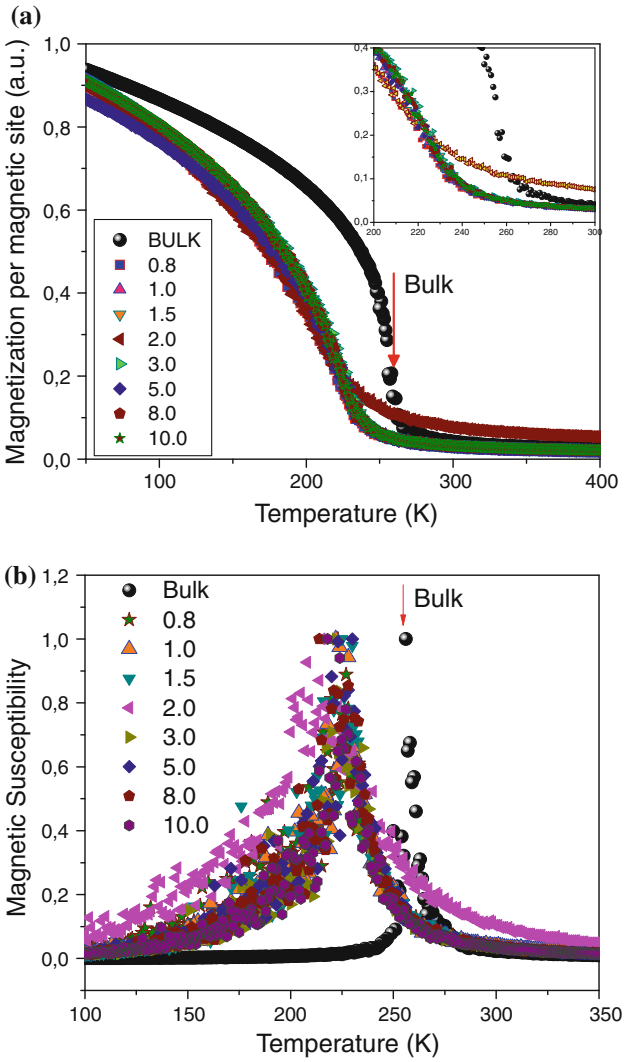

Fig. 2 Temperature dependence of **a** magnetization and **b** magnetic susceptibility at zero magnetic field cooled, for the different p metric values included in this work. Results corresponding to bulk manganite are also included for comparison. Critical temperatures are estimated from the position at the maximum of susceptibility

properties are considered along the (111) direction as easy axis for the core magnetization, whereas for surface spins, direction is determined by the single ion surface anisotropy vectors according to Eq. 2. Results corresponding to the bulk manganite, considering periodic boundary conditions, are also included for comparison. Critical temperatures, indicated by arrows and estimated from the location of the maximum of the magnetic susceptibility, reveal clearly a reduction of T_C of about 40 K relative to the bulk $T_C = 260$ K as expected. Such reduction is ascribed to the breaking of symmetry at the surface of the nanoparticles giving rise to a smaller average coordination number and consequently a smaller density of magnetic bonds respect to the bulk [23]. Results seem also to reveal insensitivity, at least for the system size considered, of the critical

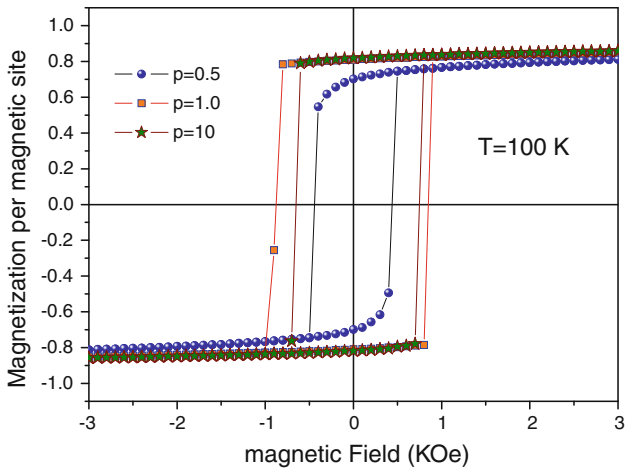

Fig. 3 Hysteresis loops for manganite nanoparticles for different metrics values and at $T = 100$ K below Curie temperature

temperature for the nanoparticles and the geometries considered. This result agrees with that obtained by Riaño-Rojas et al. [19]. As is observed, susceptibility curves do not exhibit blocking and/or freezing process, because the former is normal caused by nanoparticles system interacting between them and the second is normally due to spin-glass transitions produced by frustrated magnetic interactions that are no present here [30, 31].

Figure 3 shows hysteresis loops for some selected p parameters ($p = 0.5$, 1.0 and 10), obtained at 100 K. Hence, magnetization reversal takes place as a whole for p values greater than 1, resembling accordingly with the Stoner–Wohlfarth model. Contrary to this, for smaller metrics values, the magnetization reversal occurs in a more gradual fashion. This fact suggests differences in the internal magnetic structure depending on the metrics. Derived from the hysteresis loops, coercive force exhibits variations depending on the p parameter which are closely linked to the surface to volume ratio (N_s/N_V), as can be observed in Fig. 4. In this figure three different regimes can be identified. First, for $0 < p < 1$, N_s/N_V decreases as p increases. The nanoparticle edges are highly bent and their lengths are greater but the enclosed volume is lower as shown in Fig. 1. At $p = 1$ the nanoparticle edges are straight lines and the N_s/N_V ratio reaches a minimum value. In the second regime, for $p > 1$ the edges become curved again (in the opposite way to that observed for low p values) and the volume enclosed is higher than in the first case. Finally, as $p \to \infty$ the nanoparticle tends to a cubic shape and $N_s/N_V \to 6/6L$. These geometric characteristics are correlated with coercivity force as can be observed by comparing Fig. 4a and b from which an inverse relationship between them can be stated. In addition, results reveal a closely direct relationship of the coercive force with N_c/N_V (being N_c the number of core ions) for p

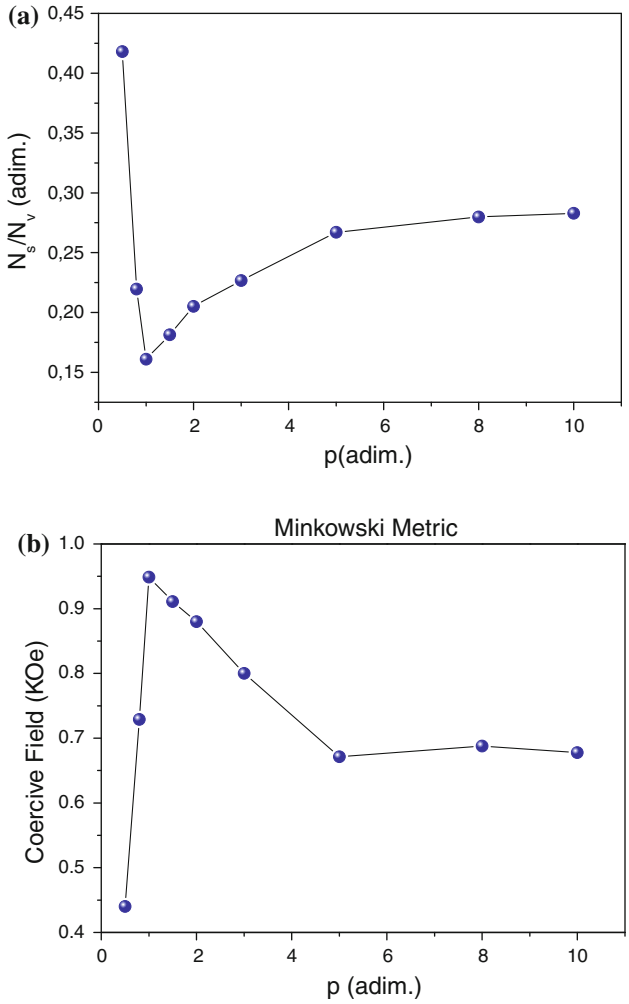

Fig. 4 Metrics dependence of **a** N_s/N_V and **b** coercive force

values above 1, according to the magnetization reversal model proposed by Stoner and Wohlfarth [32, 33]. This fact occurs because as N_s/N_V increases, the magnetic bonds density decreases due to the increasing proportion of broken bonds at the surface. Therefore, a lower applied magnetic field is in order to induce magnetization reversal [34].

Regarding electronic transport properties, resistivity as a function of temperature for several shapes generated by using the Minkowski metrics was also obtained. Figure 5a shows the resistivity as a function of temperature for different p values at zero field cooled whereas Fig. 5b shows the case at a fixed metrics and for different external applied field values. Movement of the electrons is considered perpendicular to the external applied field direction that was along the (111) direction that is the easy axis of these manganites. On the other hand, as reported by other authors, a bump is observed in ρ close to T_C [35]. In this figure two regions can be identified. First, an insulating behavior above T_C in the paramagnetic regime at the right

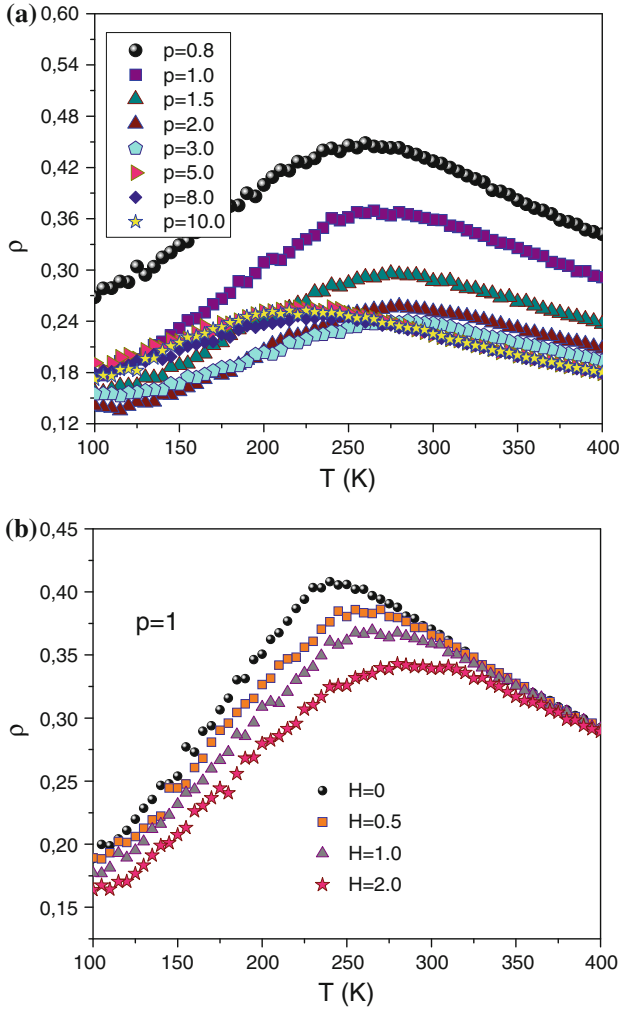

Fig. 5 **a** Zero field temperature dependence of the resistivity for different p values. **b** Temperature dependence of the resistivity at $p = 1$ for different values of the external applied field

side of the plot is found. Upon further decreasing the temperature a metallic state is obtained. Second, near T_C a fairly sharp transition in the resistivity occurs, leading to a metallic behavior in the ferromagnetic regime at the left side of the curve. On both sides of T_C, the resistivity ρ decreases exponentially [27] and the p dependence of the resistivity is evident. For lower p values, the maximum in resistivity is higher, because of the increase in the surface anisotropy and the scattering of conduction electrons is grater according to the Hund coupling [36]. Nevertheless, for $p \to \infty$ the curves do not have strong variation, because of the nanoparticles shapes are almost the same. Other important result shown in Fig. 5b is the influence of magnetic field on the resistivity [37]. A decrease in the resistivity caused by the external applied field is observed. This effect has been called magnetoresistance (MR). Magnetic fields affect drastically the electron transport properties of manganites and relatively small fields of a few Teslas induce important changes in the resistivity. These features have been also reported by Vandewalle [27]. This behavior is possible due to the fact than an external magnetic field helps spins to be oriented in its direction, favoring the Hund coupling. The phenomenology behind this behavior has been subject of study in other researches and it continues to be a matter of discussion and debate. In the literature, there are some experimental reports about magnetic properties of LCMO nanoparticles, presenting magnetization, AC susceptibility and hysteresis loops. Normally these results give information about a system of nanoparticles that some times are considered as powder with nanosize grains [38]. Although some general features are similar to those presenting here, the interaction between nanoparticles affect the magnetic properties.

Conclusions

The influence of the geometrical shape, in the framework of the Minkowski metrics on the magnetic, hysteretic and electrical transport properties of ferromagnetic manganite nanoparticles of approximately the same size was carried out. Results revealed clearly the specific way as magnetic properties become modified in a system of a rather well-defined size depending on the shape of the nanoparticles. Well-differentiated regimes depending on the metrics value were also identified. Regarding the critical properties, the Curie temperature seems to be independent on the shape of the nanoparticles having approximately the same amount of Mn ions, whereas the coercive force does exhibit a strong dependence with the metrics and the surface to volume ratio. In particular, magnetization reversal mechanisms resulted to be dependent on the metrics as well as the resistivity $p \to \infty$.

Acknowledgements The authors gratefully acknowledge the financial support of Dirección Nacional de Investigaciones of Universidad Nacional during the course of this research, under project 7785. This work was also supported in part by the GES and GICM Sustainability projects, the IN565CE, IN576CE, and IN578CE projects of the Antioquia University. One of the authors (J.R) wants also to acknowledge to the Spanish Education Ministry for the sabbatical year Grant SB2009-0210.

References

1. Bader SD (2006) Rev Mod Phys 78:1
2. Zhu J-G (2003) Mater Today 6:22
3. Zhu J-G, Park C (2006) Mater Today 9:36
4. White RL, Newt RMH, Pease RFW (1997) IEEE Trans Magn 33:990
5. Vavassori P, Donzelli O, Callegaro L, Grimsditch M, Metlushko V (2000) IEEE Trans Magn 36:2993

6. Vavassori P, Zaluzec N, Metlushko V, Novosad V, Ilic B, Grimsditch M (2004) Phys Rev B 69:214404
7. Cowburn RP, Koltsov DK, Adeyeye AO, Welland ME (1999) Europhys Lett 48(2):221
8. Hehn M, Ounadjela K, Bucher JP, Rousseaux F, Decanini D, Bartenlian B, Chappert C (1996) Science 272:1782
9. Shi J, Tehrani S, Scheinfein MR (2000) Appl Phys Lett 76:2588
10. Goll D, Schütz G, Kronmüller H (2003) Phys Rev B 67:094414
11. Koltsov DK, Welland ME (2003) J Appl Phys 94(5):3457
12. Shinjo T, Okuno T, Hassdorf R, Shigeto K, Ono T (2000) Science 289:930
13. Natali M, Prejbeanu IL, Lebib A, Buda LD, Ounadjela K, Chen Y (2002) Phys Rev Lett 88:1
14. Zhu FQ, Chern GW, Tchernyshyov O, Zhu XC, Zhu JG, Chien CL (2006) Phys Rev Lett 96:027205
15. Goolaup S, Adeyeye AO, Singh N (2006) Phys Rev B 73:104444
16. Rostamnejadi Ali, Salamati Hadi, Kameli Parviz, Ahmadvand Hossein (2009) J Magn Magn Mater 321:3126
17. Roy S, Dubenko I, Edorh DD, Ali N (2004) J Appl Phys 96:1202
18. Dey P, Nath TK (2006) Appl Phys Lett 89:163102
19. Riaño-Rojas JC, Restrepo-Parra E, Orozco-Hernández G, Restrepo J, Jurado JF, Vargas-Hernández C (2009) IEEE Trans Magn 45:5196
20. Cheong S-W, Hwang HY (1999) In: Tokura Y (ed) Colossal magnetoresistance oxides, Monographs in condensed matter science. Gordon and Breach, London
21. Miller RI, Arseneau D, Chow KH, Daviel S, Engelbertz A, Hossain MD, Keeler T, Kiefl RF, Kreitzman S, Levy CDP, Morales P, Morris GD, MacFarlane WA, Parolin TJ, Poutissou R, Saadaoui H, Salman Z, Wang D, Wei JYT (2006) Phys B Condens Matter 374–375:30
22. Hotta T, Feiguin A, Dagotto E (2001) Phys Rev Lett 86:4922
23. Mazo-Zuluaga J, Restrepo J, Mejía-López J (2007) Phys B Condens Matter 398:187
24. Christides C, Moutis N, Komninou Ph, Kehagias Th, Nouet G (2002) J Appl Phys 92:397
25. Kodama RH, Berkowitz AE (1999) Phys Rev B 59:6321
26. Otero-Leal M, Pardiñas I, Rivadulla F, Lopez-Quintela MA, Rivas J (2006) Boletin de la Sociedad española de Cerámica y Vidrio 45:175
27. Okamoto S, Ichihara S, Maekawa S (2002) Phys Rev B 65:144403
28. Kreyszig E (1989) Introductory functional analysis with applications. Wiley, USA, p 11
29. Vandewalle N, Ausloos M, Cloots R (1999) Phys Rev B 59:11909
30. Fonseca FC, Goya GF, Jardim RF, Muccillo R, Carreño NLV, Longo E, Leite ER (2002) Phys Rev B 66:104406
31. Bogner J, Reisnner M, Steiner W (1999) J Magn Magn Mater 196–197:641
32. Stoner EC, Wohlfarth EP (1948) Philos Trans R Soc Lond A 240(826):599
33. Tannous C, Gieraltowski J (2008) Eur J Phys 29:475
34. Mazo-Zuluaga J, Restrepo J, Mejía-López J (2008) J Appl Phys 103:113906
35. Bastiaansen PJM, Knops HJF (1998) J Phys Chem Solids 59:297
36. Cheong S-W, Hwang HY (1999) In: Tokura Y (ed) Colossal magnetoresistance oxides, Monographs in condensed matter science, Gordon & Breach, London
37. Dagotto E, Hotta T, Moreo A (2001) Phys Rep 344:1
38. Markovica D, Kusigerskia V, Tadica M, Blanusaa J, Jaglicic Z, Cvjeticaninc N, Spasojevic V (2010) J Alloys Compd 494:52